Synthesis of 3D Printable Cu–Ag Core–Shell Materials: Kinetics of CuO Film Removal

SEONGIK HONG[1] and NAMSOO KIM[1,2]

1.—Department of Metallurgical & Materials Engineering, The University of Texas at El Paso, 500 W. University Ave, El Paso, TX 79968-0520, USA. 2.—e-mail: nkim@utep.edu

In this research, Cu–Ag core–shell particles were synthesized as a functional and 3D printable material. Using the solid–liquid method, Cu–Ag core–shell particles were simply synthesized, and different particle sizes of 100 nm and 2 μm were used to confirm the size effect in the synthesis and reaction control of the Cu–Ag core–shell particles. In addition, highly viscous Cu–Ag core–shell particle paste was also prepared, and its electrical conductivity was measured. As a result, the reaction rate in the case of the 2 μm Cu particles was controlled by film diffusion, whereas for the 100 nm Cu particles, the reaction rate was controlled by CuO film produced before reacting with Ag ions in solution, and limited by chemical reaction control. Through the solid–liquid method, dendrite-shaped Cu–Ag core–shell particles were formed. Also, the electrical conductivity increased with increasing sintering temperature and core–shell particle concentration.

Key words: 3D printing technology, highly viscous functional materials, Cu–Ag core–shell, CuO film, interfacial limiting control

Notation

r_c	Radius of unreacted core
R	Radius of particle
t	Reaction time
$t_{comp.}$	Completed reaction time
l	Reaction order
k'	Rate constant

INTRODUCTION

Three-dimensional printing technology offers significant ability to print diverse materials, having nearly unlimited applicability in many different industrial fields worldwide. In traditional 3D printing, methods such as fused deposition modeling (FDM),[1] selective laser sintering (SLS),[2] stereolithography apparatus (SLA),[3] and electron-beam melting (EBM)[4] are used to create 3D-printed

objects using materials such as thermoplastics,[1] metal powders,[2,4] and ultraviolet (UV)-curable polymers.[3] However, traditional 3D printing can only print the materials mentioned above, thus limiting the range of application of 3D printing technology to date. To print a wider range of materials and increase the usefulness of 3D printing overall, highly viscous materials including functional materials need to be developed and adopted. By printing with highly viscous paste, a wider range of functional 3D structures can be printed using a 3D printer. In this study, core–shell particles were synthesized as a functional material for use in highly viscous printable material. Core–shell particles have special properties, including optical properties,[5] ability for drug storage and release,[6] catalytic properties for use in organic reactions,[7] specific reactivity,[8] and antimicrobial properties.[9] These unique characteristics of core–shell particles are expected to be of benefit in multiple industrial and research fields.

Currently, many methods exist for synthesis of core–shell particles; For example, spray pyrolysis,[10] the polymer shell method,[11] radical polymerization,[12] sonosynthesis,[13] and the reduction reaction method[14] have been studied. Also, to produce core–shell particles with a stable film, many additives,

precursors, and stabilizers have been used in their synthesis process.

To enable wide application of core–shell particles in multiple industries, their synthesis processes should be simple. The synthesis methods mentioned above are complicated, involving many steps and having high cost. Furthermore, if stabilizers and other additives are used to synthesize core–shell particles, additional processing steps are required to remove these materials, making the total synthesis process more complicated. Therefore, in this study, Cu–Ag core–shell particles were simply prepared using the solid–liquid method without stabilizers or additives. Because of the high conductivities of these two metals, Cu–Ag core–shell particles are applicable for printed electronics and 3D printing technology as materials for solar cells or highly viscous conductive pastes. Many studies have been conducted on the useful properties of Cu–Ag core–shell particles.[15] In this work, Cu particles and Ag ions were reacted in solution. Due to the difference in their electromotive force (EMF) values [Ag (0.799), Cu (0.337) volts SHE (standard hydrogen electrode)],[16] the Cu particle was oxidized, releasing two electrons. At the same time, Ag ions were reduced to Ag metal by the electrons released from the Cu particles to form an Ag layer on the surface of the Cu particles. In addition, 100 nm and 2 μm Cu particles were used to characterize the effect of particle size on the reaction rate during the synthesis of the Cu–Ag core–shell particles. Experiments were also carried out at different Ag ion conditions to confirm the effect of the Ag ion concentration in solution on the reaction rate during Cu–Ag core–shell particle synthesis. The resulting difference in reaction rate between the 100 nm and 2 μm particle conditions was compared and analyzed as basic research for Cu–Ag core–shell particle synthesis from the point of view of reaction rate. Furthermore, to form a highly viscous material, Cu–Ag core–shell particles were mixed with highly viscous flux, and its electrical conductivity was measured.

EXPERIMENTAL PROCEDURES

Materials

In this study, CuO was reduced to Cu metal particles and then used as Cu nanoparticles. In this experiment, 2 μm Cu particles (Nano Technology) were also used. Hydrazine monohydrate (purity ≥99%; Alfa Aesar) was used to reduce CuO, and the average particle size of the Cu nanoparticles reduced by hydrazine monohydrate was 100 nm. Silver nitrate (purity ≥99.8%; Sigma Aldrich) was used as the source of Ag ions in solution.

Synthesis and Analysis of Cu–Ag Core–Shell Particles

In this study, the Cu concentration was fixed but the Cu particle size and the Ag concentration were experimental variables. All experiments were performed at room temperature. The synthesis process was as follows: First, 50 mL 1×10^{-1} mol dm^{-3} Cu particle solution was prepared by mixing 100 nm Cu particles with distilled water. Next, Ag ion solutions were prepared where the Ag concentration differed for each experiment with values of 1×10^{-2} mol dm^{-3}, 5×10^{-2} mol dm^{-3}, 1×10^{-1} mol dm^{-3}, 1.5×10^{-1} mol dm^{-3}, 2×10^{-1} mol dm^{-3}, and 4×10^{-1} mol dm^{-3}. When the Cu solution and Ag ion solutions were mixed in each experiment, their concentration changed because the total volume of solution changed from 50 mL to 100 mL. Therefore, the concentration of Cu became 5×10^{-2} mol dm^{-3} in the mixed solution while that of Ag ions in solution became 5×10^{-3} mol dm^{-3}, 2.5×10^{-2} mol dm^{-3}, 5×10^{-2} mol dm^{-3}, 7.5×10^{-2} mol dm^{-3}, 1×10^{-1} mol dm^{-3}, and 2×10^{-1} mol dm^{-3} in the 100 mL solution for each experiment. After combining the two solutions, the mixture was stirred at 300 rpm and reacted for 10 min. The mixture was then subjected to centrifugation at 6000 rpm for 10 min to separate the Cu–Ag core–shell particles from solution. After the centrifugation process was complete, the Cu–Ag core–shell particles were washed with distilled water. The rinse water and core–shell mixture were then subjected to a centrifugation process again using the same conditions as before. Finally, the core–shell particles were dried in a vacuum oven at 80°C. Experiments involving 2 μm Cu particles were performed using the same process as described above. Each sample was analyzed by inductively coupled plasma (ICP, Optima 7000 DV; PerkinElmer) and scanning electron microscopy (SEM; TM-1000 tabletop microscope, Hitachi; S-4800 scanning electron microscopy, Hitachi).

The prepared Cu–Ag core–shell particles were mixed with highly viscous flux to form Cu–Ag core–shell particle paste. To confirm the effect on the conductivity of the paste, the content of core–shell particles in the paste was changed from 19 vol.% to 31 vol.%. The paste was heat-treated in a furnace (Box furnace, Lindberg/Blue M) at 500°C for 20 min. In addition, the heat-treatment temperature was also changed from 400°C to 550°C to confirm the effects of this temperature on the paste. The electrical conductivity of heat-treated samples was measured using a four-pin probe (LORESTA-GP MCP-T610; Mitsubishi Chemical Corporation).
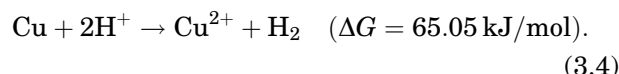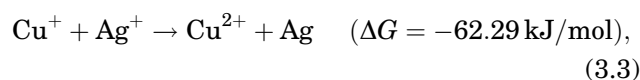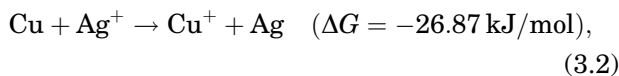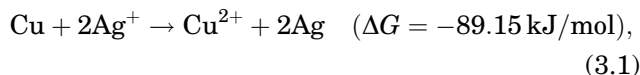
RESULTS AND DISCUSSION

Cu Particle Size Effect on Reaction Rate

In this study, Cu–Ag core–shell particles were synthesized by using 2 μm and 100 nm Cu particles without any additives or stabilizers. The concentration of the Cu ions produced was measured by ICP analysis, and the change in concentration of Cu ions at 2 μm Cu conditions is shown in Fig. 1.

Based on Fig. 1, it is confirmed that the reaction completed between 5 s and 10 s for the 2 μm Cu particle condition for all the Ag ion concentrations. In Fig. 1, it is observable that the concentration of

the Cu ions produced and the reaction rate increased as the Ag ion concentration was increased. The reaction rate was calculated as well as the order of the reaction based on the changes of the Cu ion concentration. In this experiment, four reactions occurred in solution according to the following equations:

$$Cu + 2Ag^+ \rightarrow Cu^{2+} + 2Ag \quad (\Delta G = -89.15\,\text{kJ/mol}),$$
$$(3.1)$$

$$Cu + Ag^+ \rightarrow Cu^+ + Ag \quad (\Delta G = -26.87\,\text{kJ/mol}),$$
$$(3.2)$$

$$Cu^+ + Ag^+ \rightarrow Cu^{2+} + Ag \quad (\Delta G = -62.29\,\text{kJ/mol}),$$
$$(3.3)$$

$$Cu + 2H^+ \rightarrow Cu^{2+} + H_2 \quad (\Delta G = 65.05\,\text{kJ/mol}).$$
$$(3.4)$$

When calculating the Gibbs free energy, the reaction described by Eq. 3.1 is the predominant reaction as compared with the other reactions, occurring in solution as shown in Fig. 2.

Therefore, Eqs. 3.2 and 3.3 are not considered. In addition, because of its Gibbs free energy, Eq. 3.4 cannot occur, meaning that hydrogen ions cannot influence this reaction. The concentration of Cu $(5 \times 10^{-2}\,\text{mol dm}^{-3}, 100\,\text{mL})$ was fixed in the reaction equation above; therefore, the Cu concentration can be considered as a rate constant in this rate equation. The rate equation can be expressed as follows:

$$\frac{d\{Cu^{2+}\}}{dt} = k'\{Ag^+\}^l. \quad (3.5)$$

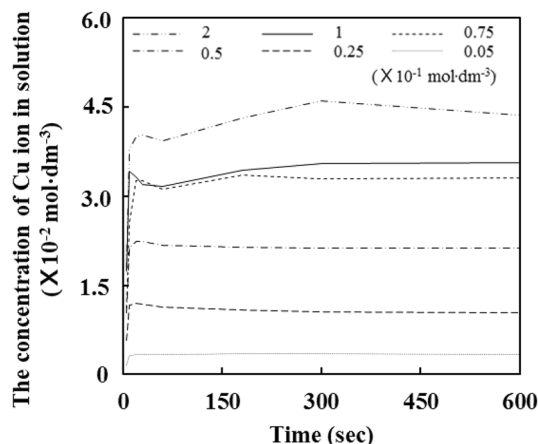The order of the reaction for each condition was calculated and is plotted in Fig. 3.

The order of the reaction was determined to be 0.65 for the 2 μm Cu particle condition. To confirm the rate-limiting step of the reaction at this condition, the shrinking core model was applied in this work. Analysis of the conversion-time curve was used to confirm the rate-limiting step of this reaction.[17] In Fig. 4, the conversion-time curve is shown and compared with the theoretical curve.

When the conversion-time curve plot (generated from experimental data) is compared with the theoretical curve in Fig. 4, the tendency of the 2 μm Cu particle curve is the same as the film diffusion control curve. Seemingly, the reaction rate of 2 μm Cu particles is limited by film diffusion control. Figure 5 shows the change in the concentration of Cu ions produced in experiments involving 100 nm Cu particles.

According to Fig. 5, the reaction was continuous when 100 nm Cu particles were used. Interestingly, as shown in Fig. 1, the reaction finished quickly when 2 μm Cu particles were used, but in the case of experiments involving 100 nm Cu particles, the reaction did not finish quickly. Generally, when particles are of a small size, the reaction rate will increase because the surface area will increase too. However, a 100 nm particle is 20 times smaller than a 2 μm Cu particle, and yet the reaction rate in the 100 nm Cu condition was slower than that in the 2 μm Cu condition. This result occurs due to the presence of CuO film on the surface of the 100 nm Cu particles. Nanosized Cu particles can oxidize easily in an ambient environment. According to previous research, to prevent oxidation of Cu nanoparticles, the oxygen pressure should be controlled at 2.6×10^{-45} atm in air.[16] Controlling such an oxygen pressure is impossible, meaning that oxidation of Cu nanoparticles cannot be prevented in air. Based on this result, it seems that, when 100 nm Cu particles are prepared to synthesize Cu–Ag core–shell particles, the surface of the Cu nanoparticles is oxidized and, at the same time, CuO film is formed on the surface before the 100 nm Cu particles can react with the Ag ion solution. Through SEM and energy-dispersive spectroscopy (EDS) analysis, it was confirmed that the 100 nm Cu particles were already oxidized to about 2 wt.%,
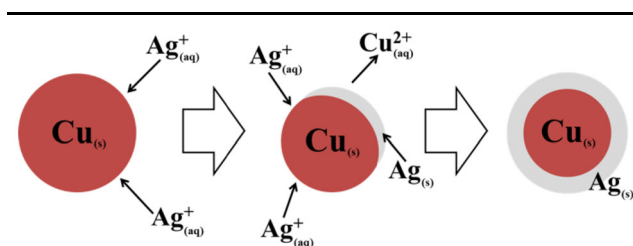

Fig. 1. Concentration of Cu ions in solution at different Ag ion concentrations (2 μm Cu particle condition).

Fig. 2. Synthesis reaction of Cu–Ag core–shell particles in aqueous solution.

Fig. 3. Plot of log(rate) versus log({Ag$^+$}) in the 2 μm Cu particle condition.
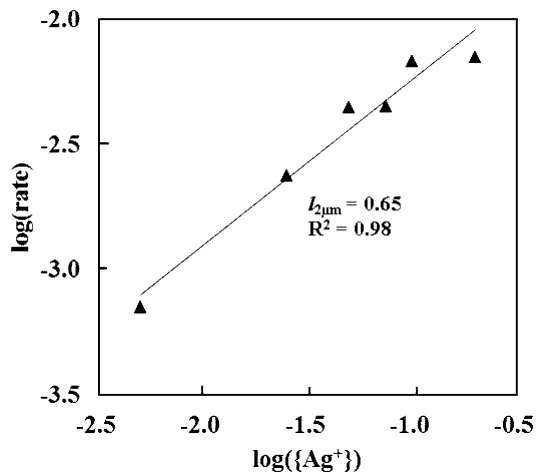
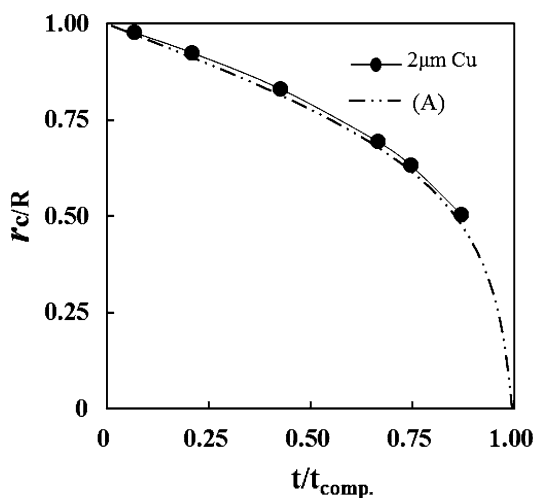Fig. 5. Cu ion concentration in solution for different Ag ion concentrations (100 nm Cu particle condition).

Fig. 4. Empirical conversion-time curve at 2 μm Cu particle condition, (A) theoretical film diffusion control conversion-time curve.

Fig. 6. SEM images and EDS analysis results of (a) 2 μm and (b) 100 nm Cu particles.

whereas the 2 μm Cu particles were not. The EDS and SEM results for the 2 μm and 100 nm Cu particles are shown in Fig. 6.

The stability of the CuO film was checked based on the Pilling–Bedworth ratio, R_{PB}.[18] The R_{PB} value for CuO is 1.6. Thus, CuO film is a stable and passivating film capable of providing a protective effect. For this reason, Ag ions cannot diffuse to the Cu through the CuO film formed on the surface of the 100 nm Cu particles.

In this condition, the pH of the solution is between 4.67 and 5.89 for Ag ion concentration between 2×10^{-1} mol dm^{-3} and 5×10^{-3} mol dm^{-3}. The surface charge of CuO is positive in this pH range,[19] so Ag ions are not absorbed onto the surface of the CuO film. Therefore, in this condition, the reaction described by Eq. 3.1 can occur and another reaction can occur in the solution as described by the following equation:
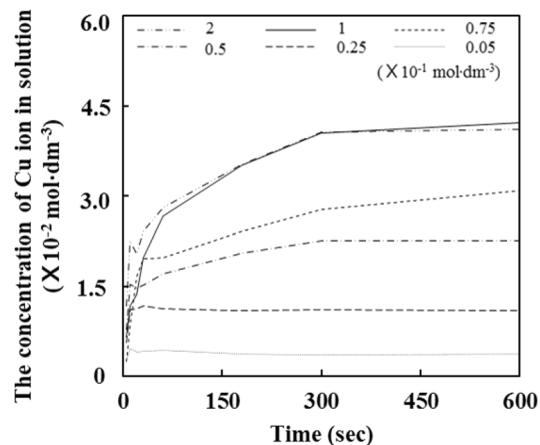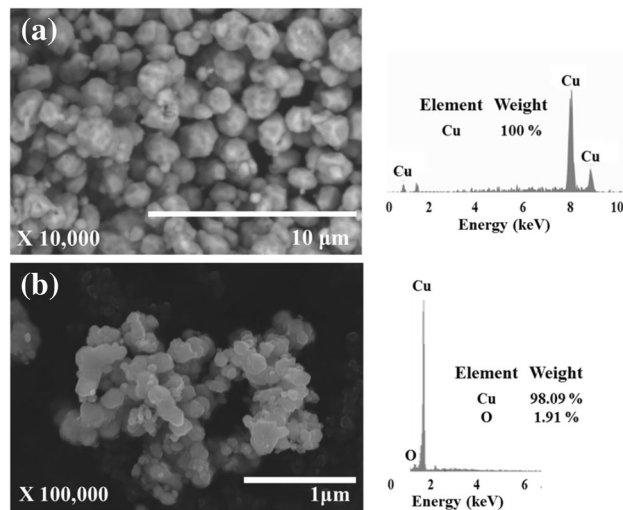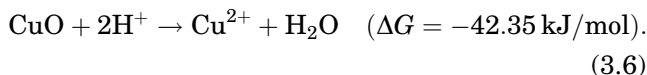
$$CuO + 2H^+ \rightarrow Cu^{2+} + H_2O \quad (\Delta G = -42.35 \, kJ/mol).$$
$$(3.6)$$

In this case, it can be considered that Eq. 3.4 cannot occur because of its Gibbs free energy. Because of the low pH condition, the CuO film reacts with acid in the solution, and so CuO releases Cu ions into solution (Eq. 3.6). At this time, a pure Cu surface will be exposed, and Ag ions and the newly exposed Cu surface can then react in solution, allowing a Ag film to be coated onto the Cu surface (Eq. 3.1). This reaction occurs continuously, and finally Cu–Ag core–shell particles are synthesized in solution. Figure 7 shows a schematic of this reaction.

Roughly 2 wt.% of the Cu was oxidized, but it was not partially oxidized. Because all the 100 nm Cu particles were oxidized to 2 wt.% to form CuO film,
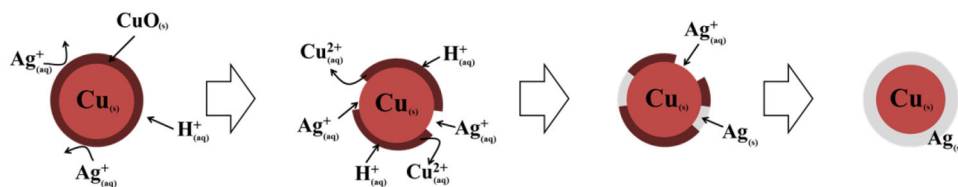
Fig. 7. Schematic of the Cu–Ag core–shell particle synthesis process using 100 nm Cu particles.
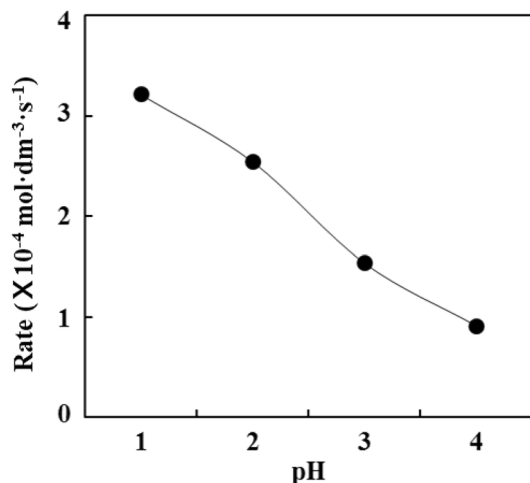

Fig. 8. pH dependence of reaction rate for 100 nm Cu particle condition.

the reaction using 100 nm Cu particles was slower than that using 2 μm Cu particles, which were not oxidized. To synthesize Cu–Ag core–shell particles using 100 nm Cu particles, the CuO film must first be removed. In this reaction, the pH of the solution could influence the reaction (Eq. 3.5). Therefore, the total reaction rate is limited by the reaction between the CuO film and hydrogen ions in solution. To increase the reaction rate in this condition, the CuO film should be removed quickly, and pH control can be used to dissolve the CuO film. The reaction rate of Eq. 3.5 was measured at different pH conditions, and the results are shown in Fig. 8.

Figure 8 confirms that, as the pH of the solution decreases, the reaction rate of Eq. 3.6 increases. In addition, it was considered that the Ag ion concentration in solution cannot influence this reaction rate because, when the 2 μm particle size was applied, the reaction finished quickly. As a result, the rate equation can be expressed as follows:

$$\frac{d\{Cu^{2+}\}}{dt} = k'\{H^+\}^l. \quad (3.7)$$

The order of the reaction was also calculated to be ~0.2 ($R^2 = 0.97$) for the 100 nm Cu particle condition. This reaction is that of CuO on the surface of 100 nm Cu particles reacting with hydrogen ions in solution. Product layer control cannot limit this reaction rate because the reaction occurs on the surface. Thus, it can be expected that Eq. 3.6 will be governed by film diffusion control or chemical reaction control. To confirm which limiting step is truly controlling this reaction rate, analysis of the conversion-time curve was again used, comparing the experimental with the theoretical curve as shown in Fig. 9.

As shown in Fig. 9, the tendency of the conversion-time curve behavior for Eq. 3.6 is the same as the conversion-time curve for chemical reaction control. Therefore, when 100 nm Cu particles were used to synthesize Cu–Ag core–shell particles, the entire reaction rate is controlled by Eq. 3.6. In addition, the reaction rate of Eq. 3.6 is limited by chemical reaction control.

When the Ag ion concentration was 1×10^{-1} mol dm^{-3} and 2×10^{-1} mol dm^{-3}, as seen in Fig. 5, the concentration of Cu ions produced in solution was the same for these concentrations. For the 2 μm Cu particle condition, as seen in Fig. 3, as the Ag ion concentration was increased, the concentration of Cu ions produced also increased. However, for the 100 nm Cu particle condition, as seen in Fig. 6, when the Ag ion concentration was under 1×10^{-1} mol dm^{-3}, the concentration of Cu ions produced increased as the Ag ion concentration was increased. This means that a stable Cu–Ag core–shell structure, which does not react with Ag ions in solution, was synthesized when 100 nm Cu particles were used with the 1×10^{-1} mol dm^{-3} Ag ion concentration. If Cu–Ag core–shell particles synthesized using the 1×10^{-1} mol dm^{-3} Ag ion concentration are stable, the concentration of Cu ions produced at conditions with higher Ag ion concentration should remain the same as for the 1×10^{-1} mol dm^{-3} condition. To confirm this, Cu–Ag core–shell particles were synthesized at higher Ag ion concentrations; the results are shown in Fig. 10.

In the case of 100 nm Cu particles, the Cu ion concentration did not increase at 1×10^{-1} mol dm^{-3} to 6×10^{-1} mol dm^{-3}, and the Cu ion concentrations measured at different Ag ion concentrations were similar. However, the Cu ion concentration increased between the 1×10^{-1} mol dm^{-3} and 2×10^{-1} mol dm^{-3} conditions for the 2 μm Cu particles, and the other results were similar to those observed for the 100 nm Cu particle condition. Therefore, stable Cu–Ag core–shell particles could be synthesized using 100 nm Cu particles with 1×10^{-1} mol dm^{-3} of Ag ions, or using 2 μm particle size with 2 ×
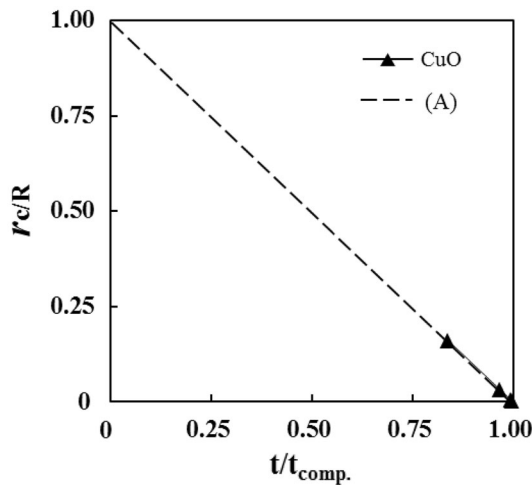
Fig. 9. Empirical conversion-time curve at 100 nm Cu particle condition, (A) theoretical chemical reaction control conversion-time curve.
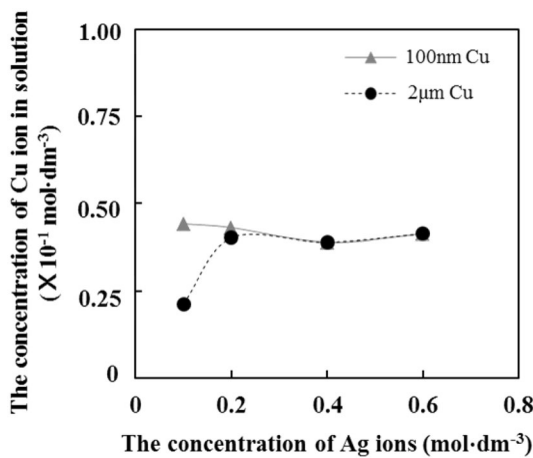

Fig. 11. SEM images and EDS results of Cu–Ag core–shell particles synthesized using (a) 2 μm and (b) 100 nm Cu particles.

Fig. 10. Change of Cu ion concentration with increasing Ag ion concentration.

Fig. 12. Conductivity of Cu–Ag core–shell particle pastes synthesized with different core–shell particle contents.

10^{-1} mol dm^{-3} of Ag ions. This result confirms that, when the Ag ion concentration is 1×10^{-1} mol dm^{-3}, the Cu–Ag core–shell particles synthesized in the 2 μm Cu particle condition were less stable compared with those formed in the 100 nm Cu particle condition, because the Cu ion concentration in solution increased as the Ag ion concentration was increased.

Shape of Cu–Ag Core–Shell Particles

SEM images of the Cu–Ag core–shell particles prepared using 2 μm and 100 nm Cu particles were also taken to confirm their morphology (Fig. 11).

Comparing the SEM micrographs for the two particle size conditions in Fig. 11, it is notable that the morphology of the synthesized core–shell particles was spherical for the 2 μm Cu particle size condition, but when 100 nm Cu particles were applied, the synthesized Cu–Ag core–shell particles exhibited dendritic structure. Disk-shaped Cu–Ag
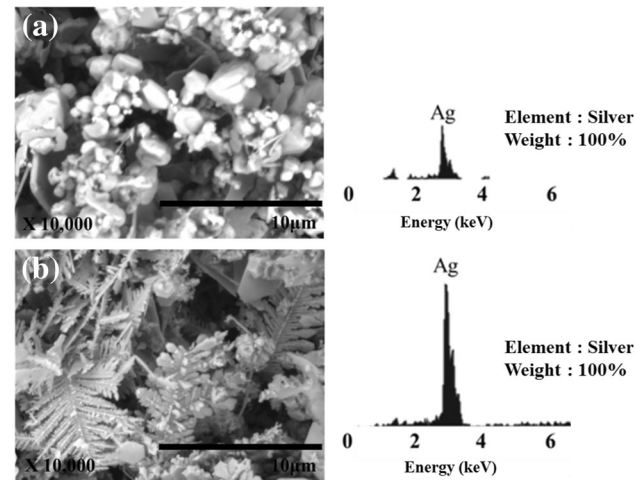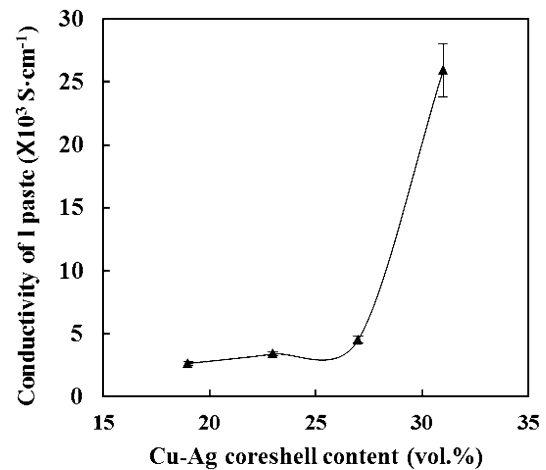
core–shell particles were also observed in both conditions.

The difference in the shape of the formed Cu–Ag core–shell particles results from the different reaction rates, affected by the existence of the CuO film on their surface. In fact, the reaction rate of the 2 μm Cu particles was much faster than that for the 100 nm particle condition. In the 2 μm Cu particle condition, Ag metal rapidly covers the surface of the Cu particles because the 2 μm Cu particles have no CuO film on their surface, so that Ag ions in the solution can react quickly without any obstacles. Because of this rapid reaction rate, the Cu–Ag core–shell particles had no time or chance to grow and formed a specific shape. Therefore, the Cu–Ag core–shell particles were formed with the most stable, spherical shape in the 2 μm Cu particle condition.

The reaction rate in the 100 nm Cu particle condition was relatively slower than that for the 2 μm Cu particle condition because of the existence of the

CuO film on the surface of the Cu nanoparticles. Therefore, when Ag ions reacted with the Cu nanoparticles, the Ag ions approached the Cu surface and were hindered by the CuO film. The CuO film slowly dissolved and was removed by reaction with the acid in the solution, leading to exposure of the Cu surface. At that time, Ag ions could react with the pure Cu surface. During this reaction, the Ag ions grew continuously, having sufficient time to produce a dendritic shape on the Cu surface. This was possible because this reaction is controlled by the CuO film on the surface of the Cu nanoparticles. This result confirms that, even though the same method was used to synthesize the Cu–Ag core–shell particles, their shape could be changed according to the reaction rate controlled by the CuO film and particles.

Electrical Conductivity Measurements

The conductivity of the Cu–Ag core–shell particles was measured using a four-pin probe. Cu–Ag core–shell particle paste was synthesized, and its particle content was changed. Figure 12 shows the results of these conductivity measurements.

The conductivity of the core–shell particle paste increased as the content of core–shell particles in the paste increased. In addition, the conductivity at 31 vol.% was 10 times higher than the conductivity at 19 vol.%. This paste had 4% of the conductivity of bulk silver metal (6.3×10^5 S cm^{-1}).[20] In this experiment, the maximum content which could be mixed with the highly viscous flux was 31 vol.%, after which more core–shell particles could not be mixed. To increase the conductivity of the paste, the sintering temperature was changed with the particle content fixed at the highest value of 31 vol.%. The conductivity results for pastes sintered at different temperatures are shown in Fig. 13.

The conductivity of the core–shell particle paste increased as the sintering temperature was increased. This means that the core–shell particles were more connected to each other at higher sintering temperature, allowing higher conductivity than for the other conditions regardless of the constant particle content in the pastes. The conductivity was 7% of that of bulk Ag metal at the highest sintering temperature condition. The surfaces of the
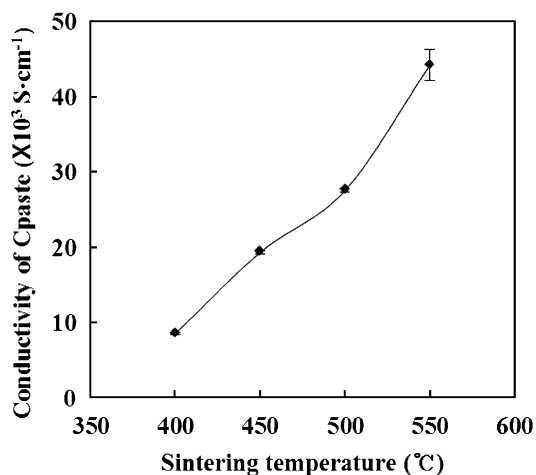

Fig. 13. Conductivity of Cu–Ag core–shell particle pastes sintered at different temperatures.
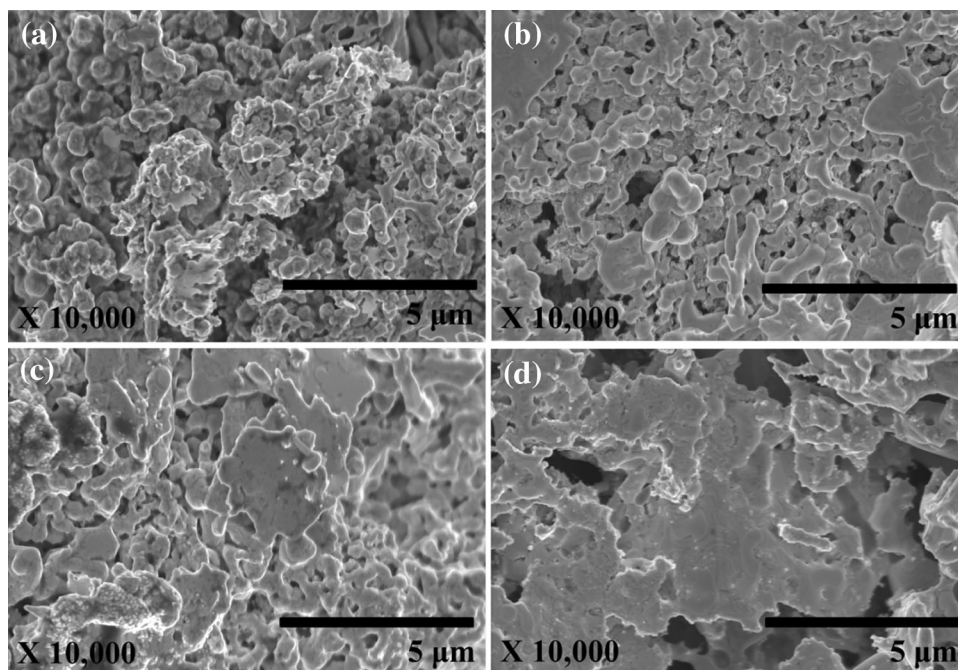

Fig. 14. SEM images of Cu–Ag core–shell particle pastes sintered at different temperatures of (a) 400°C, (b) 450°C, (c) 500°C, and (d) 550°C.

sintered core–shell particle pastes are shown in Fig. 14.

According to Fig. 14, at the low temperatures of 400°C and 450°C, most particles were melted. The core–shell particles were not perfectly connected to each other, just exhibiting a small neck between them. However, in the other conditions of 500°C and 550°C, the particles were better connected, and most of them were melted and fused, forming a thin layer. Such a thin layer could be observed for all the temperature conditions but was better formed and observable as the sintering temperature was increased. So, to form a thin, more consistent layer of Cu–Ag core–shell particles, a higher sintering temperature condition is required. Also, the conductivity of the paste increased as the sintering temperature was increased, despite the visual appearance of a porous or even cracked surface.

CONCLUSIONS

In this study, Cu–Ag core–shell particles were synthesized using Cu particles of different sizes (2 μm and 100 nm). It was confirmed that the reaction in the 2 μm Cu particle condition is controlled by film diffusion control, whereas the reaction in the 100 nm Cu particle condition was controlled by the CuO film on the surface of the 100 nm Cu particles. The reaction rate in the case of the 100 nm Cu particle condition was limited by the reaction of the CuO film with acid in solution to release Cu ions. The reaction of CuO with hydrogen ions in solution is controlled by chemical reaction control. The shape of the Cu–Ag core–shell particles synthesized using different conditions was confirmed. The Cu–Ag core–shell particles obtained using 2 μm Cu particles possessed spherical morphology, whereas those obtained using 100 nm Cu particles possessed dendritic structure. The conductivity of the Cu–Ag core–shell particle paste increased as the content of Cu–Ag core–shell particles in the paste was increased. The conductivity for the highest particle content was 10 times higher than that for the lowest content. In this case, however, the conductivity was 4% of the conductivity of bulk silver. As the sintering temperature was increased, the conductivity also increased. The conductivity for the highest sintering temperature condition was 4.6 times higher than that for the lowest condition. In this case, the conductivity of the core–shell particle paste was 7% of the conductivity of bulk Ag metal. To further increase its conductivity, research into the development of highly viscous flux that can be mixed with higher contents of core–shell particles should be performed.

REFERENCES

1. D. Croccolo, M.D. Agostinis, and G. Olmi, *Comput. Mater. Sci.* 79, 506 (2013).
2. F. Xie, X. He, S. Cao, and X. Qu, *J. Mater. Process. Technol.* 213, 838 (2013).
3. A. Bertsch, H. Lorenz, and P. Renaud, *Sens. Actuators A Phys.* 73, 14 (1999).
4. J. Hernandez, S.J. Li, E. Martinez, L.E. Murr, X.M. Pan, K.N. Amato, X.Y. Cheng, F. Yang, C.A. Terrazas, S.M. Gaytan, Y.L. Hao, R. Yang, F. Medina, and R.B. Wicker, *J. Mater. Sci. Technol.* 29, 1011 (2013).
5. B. SaraswathiAmma, K. Manzoor, K. Ramakrishna, and M. Pattabi, *Mater. Chem. Phys.* 112, 789 (2008).
6. X. Chen, *Colloids Surf. A* 428, 79 (2013).
7. Z. Zhang, H. Che, Y. Wang, J. Gao, Y. Ping, Z. Zhong, and F. Su, *Chem. Eng. J.* 211, 421 (2012).
8. N. Singh, A. Ponzoni, R.K. Gupta, P.S. Lee, and E. Comini, *Sens. Actuators B Chem.* 160, 1346 (2011).
9. A.M. Abdel-Mohsen, R.M. Abdel-Rahman, R. Hrdina, A. Imramovský, L. Burgert, and A.S. Aly, *Int. J. Biol. Macromol.* 50, 1245 (2012).
10. K.C. Pingali, S. Deng, and D.A. Rockstraw, *Powder Technol.* 183, 282 (2008).
11. M. Ghahari, P. Fabbri, F. Pilati, L. Pasquali, M. Montecchi, and R. Aghababazadeh, *Ceram. Int.* 39, 4513 (2013).
12. H.S. Hwang, J.H. Bae, H.G. Kim, and K.T. Lim, *Eur. Polym. J.* 46, 1654 (2010).
13. N. Ghows and M.H. Entezari, *Ultrason. Sonochem.* 19, 1070 (2012).
14. R. Feng, M. Li, and J. Liu, *Colloids Surf. A* 406, 6 (2012).
15. H.T. Hai, H. Takamura, and J. Koike, *J. Alloys Compd.* 564, 71 (2013).
16. K.N. Han and N.S. Kim, *Kona Powder Part. J.* 27, 74 (2009).
17. O. Levenspiel, *Chemical Reaction Engineering*, 3rd ed. (New York: Wiley, 1999), pp. 566–588.
18. C. Xu and W. Gao, *Mater. Res. Innov.* 3, 231 (2000).
19. J.A. Lewis, *J. Am. Ceram. Soc.* 83, 2341 (2000).
20. K.S. Kim and K.N. Han, *J. Appl. Phys.* 108, 102801 (2010).